Neurological Sciences
https://doi.org/10.1007/s10072-019-04229-z

ORIGINAL ARTICLE

Impact of brain atrophy on tDCS and HD-tDCS current flow: a modeling study in three variants of primary progressive aphasia

Gozde Unal[1] · Bronte Ficek[2] · Kimberly Webster[2,3] · Syed Shahabuddin[1] · Dennis Truong[1] · Benjamin Hampstead[5] · Marom Bikson[1] · Kyrana Tsapkini[2,4]

Received: 14 September 2019 / Accepted: 24 December 2019

Abstract

Background During transcranial direct current stimulation (tDCS), the amount and distribution of current that reaches the brain depends on individual anatomy. Many progressive neurodegenerative diseases are associated with cortical atrophy, but the importance of individual brain atrophy during tDCS in patients with progressive atrophy, including primary progressive aphasia (PPA), remains unclear.

Objective In the present study, we addressed the question whether brain anatomy in patients with distinct cortical atrophy patterns would impact brain current intensity and distribution during tDCS over the left IFG.

Method We developed state-of-the-art, gyri-precise models of three subjects, each representing a variant of primary progressive aphasia: non-fluent variant PPA (nfvPPA), semantic variant PPA (svPPA), and logopenic variant PPA (lvPPA). We considered two exemplary montages over the left inferior frontal gyrus (IFG): a conventional pad montage (anode over F7, cathode over the right cheek) and a 4 × 1 high-definition tDCS montage. We further considered whether local anatomical features, specifically distance of the cortex to skull, can directly predict local electric field intensity.

Results We found that the differences in brain current flow across the three PPA variants fall within the distribution of anatomically typical adults. While clustering of electric fields was often around individual gyri or sulci, the minimal distance from the gyri/sulci to skull was not correlated with electric field intensity.

Conclusion Limited to the conditions and assumptions considered here, this argues against a specific need to adjust the tDCS montage for these patients any more than might be considered useful in anatomically typical adults. Therefore, local atrophy does not, in isolation, reliably predict local electric field. Rather, our results are consistent with holistic head anatomy influencing brain current flow, with tDCS producing diffuse and individualized brain current flow patterns and HD-tDCS producing targeted brain current flow across individuals.

Keywords HD-tDCS · Conventional tDCS · Primary progressive aphasia · Electrical current flow · Modeling · Atrophy

✉ Kyrana Tsapkini
tsapkini@jhmi.edu

[1] Department of Biomedical Engineering, The City College of New York, New York, NY 10031, USA

[2] Department of Neurology, Cerebrovascular Division, Johns Hopkins Medicine, 600 N. Wolfe Street, Phipps 488, Baltimore, MD 21287, USA

[3] Department of Otolaryngology, Johns Hopkins Medicine, Baltimore, MD 21287, USA

[4] Department of Cognitive Science, Johns Hopkins Medicine, Baltimore, MD 21218, USA

[5] Department of Psychiatry, University of Michigan, Ann Arbor, MI 48109, USA

Introduction

The current flow pattern through the head during transcranial direct current stimulation (tDCS) is determined by both the electrode montage (dose [1]) and anatomy [2, 3]. Therefore, the same tDCS dose delivered to different individuals results in distinct current flow patterns, as shown by computational current flow models [4–9] and experiments [10–13]. Individual differences may be amplified in cases of atypical anatomy, including skull defects [14, 15], brain injury such as stroke [16–19], aging [20, 21], or brain atrophy characteristic of several neurodegenerative disorders [22]. The ability of tDCS to enhance language neurorehabilitation in post-stroke aphasia as well as primary progressive aphasia (PPA) (see [23, 24] for results of large clinical

Published online: 10 February 2020

trials in post-stroke and PPA, respectively) is broadly investigated.

PPA is a syndrome comprising three main variants, each with its own pattern of atrophy [25, 26]. Briefly, non-fluent variant PPA (nfvPPA) shows atrophy over the left frontal lobe, semantic variant PPA (svPPA) shows atrophy over the temporal lobes bilaterally, mostly in the left (LH) rather than in the right hemisphere (RH), and logopenic variant PPA (lvPPA) shows atrophy over left posterior parietal and temporal lobes. A recent study by Cotelli and colleagues [27] showed that local brain atrophy in specific brain areas related to the therapy task (oral naming) correlated with tDCS effects on oral naming in nfvPPA. Our group demonstrated the same association between local brain atrophy and tDCS effects in trained and untrained items for tDCS coupled with written naming and spelling therapy [28]. In addition, we showed differential tDCS effects in each variant. However, the question that still remains is whether the variant-distinct atrophy patterns affect electrical current distribution. The present study addresses this question. If it is the case, then variant-distinct current distribution may moderate variant-distinct tDCS effects. If it is not the case, then variant-distinct current distribution may not moderate variant-distinct tDCS effects.

There is only one study on svPPA, previously known as semantic dementia, that has taken hypothesized atrophy of the stimulated areas into account for electrode placement, but used synthetic models (rendered on a standard head), not individual patients' models of the stimulated areas (left or right temporal lobes) [22]. If variant-distinct current distribution affects tDCS effects, they should be taken into consideration when applying tDCS in patients with different atrophy patterns.

In the present study, we directly addressed the question of whether the different patterns of atrophy in the three variants of PPA result in different current flow distribution. Answering this question has important theoretical and clinical implications because if atrophy patterns affect current flow, they should be taken into consideration by the clinician and the clinical researcher to optimize tDCS targets. We selected three exemplary subjects with substantially distinct atrophy patterns, each corresponding to one of the three main variants of PPA, to test for relationships between local atrophy and resulting electrical current flow in the brain. Analysis was focused on a single exemplary montage targeting the left inferior frontal gyrus (IFG) with an active anode of 5 × 5 cm electrodes and an extracephalic cathode (F7-right cheek) used in our clinical trial of tDCS in PPA [24]. In addition, we simulated a focal 4 × 1 HD-tDCS montage. We applied previously experimentally verified model assumptions [10–13] in state-of-the-art segmentation of the brain with atrophy. We further compared quantifiable local features of anatomy (minimum brain to skull distance, further segregated into minimum sulci- or gyri-skull distance) with local electric field magnitude and direction [29].

Methods

Informed consent was obtained from all individual participants included in the study. The pipeline of the modeling process includes segmenting the MRI into different tissue compartments, assigning conductivity to each compartment, placing virtual electrodes on the models, turning the volumetric anatomy into a 3D mesh and numerically solving the Laplace equation for the voltage distribution on this finite element model (FEM) [5]. Images from three subjects, each representing a variant of primary progressive aphasia (PPA), i.e., non-fluent variant PPA (P1_nfvPPA), semantic variant PPA (P2_svPPA), and logopenic variant PPA (P3_lvPPA), were collected. For clinical and demographic characteristics, see Table 1. T1- and T2-weighted sequence MRIs were collected at 1-mm resolution at the Kennedy Krieger Institute at Johns Hopkins University with a 3T Philips Achieva MRI scanner with a 32-channel head coil. T1-weighted scans were acquired sagittally for 5.5 min (159 slices, isotropic 1-mm voxel size, flip angle of 8°, SENSE acceleration factor of 2; TR/TE = 8/3.7 ms). T2-weighted scans were acquired in axial orientation and lasted about 3 min (70 slices, voxel size 0.828 × 0.828 × 2.2 mm, flip angle of 90°, TR/TE = 4200/12 ms).

The three subjects' images, which have different patterns of atrophy, were segmented into six tissue compartments adapting the automated algorithm ROAST [30]. Segmentation initiated with SPM8 (the New Segment routine, see [31, 32] for details) and automatic touch-up on the segmentation results were performed by morphological operations [32]. Residual errors were patched by manual segmentation techniques using ScanIP (Simpleware Version N-2018.03; Synopsys Inc., Mountain View, USA). Manual segmentation was completed by two independent expert technicians per image and a third expert technician addressed mismatches.

The segmented layers (with respective electrical conductivities, σ) were the skin (σ = 0.465 S/m), skull (σ = 0.01 S/m), gray matter (σ = 0.276 S/m), white matter (σ = 0.126 S/m), cerebrospinal fluid (σ = 1.65 S/m), and air (σ = 1e-15 S/m). We did not consider changes in properties of intact but atrophied tissue. A realistic rendered model of sponge and electrodes were embedded to the target and a mesh was generated. The mesh was imported into COMSOL and assigned conductivities based on the different domains in the mesh. Boundary conditions were assigned to regulate current density. The Laplace equation $\nabla \cdot (\sigma \nabla V) = 0$ (V, potential; σ, conductivity) was solved and the boundary conditions used were (1) inward current flow = Jn (normal current density) applied to the distal surface of the "anode" electrode(s), (2) ground

Table 1 Clinical and demographic characteristics of participants. Standard high school education is 12 years. Years post disease onset was self-reported. Language and total severity come from the Frontotemporal Dementia Clinical Dementia Rating Scale [34]. Letter fluency is sum of words generated starting with F, A, and S in 1 min per letter; semantic fluency is sum of fruits, animals, and vegetables in 1 min per category [69]. Digit and spatial spans are the numbers of digits correctly repeated—in the case of half points, one of two trials of each length of digits was correctly repeated [70]. Sentence anagrams are an in-house task developed at Johns Hopkins University. The sentence repetition task is part of the National Alzheimer's Coordinating Center packet (NACC UDS-FTLD Neuropsychol. Battery Instr. Form C1-F. 3.0, Washington: University of Washington; 2015). The Boston Naming Test represents ability to name objects with a range of frequencies [71]; its counterpart, the Hopkins Assessment for Naming Actions, represents ability to name actions [72]. S.O.A.P. refers to the subject-relative, object-relative, active, passive comprehension test [73]

ID	P1_nfvPPA	P2_svPPA	P3_lvPPA
PPA variant	Non-fluent	Semantic	Logopenic
Education (years)	18	18	18
Sex	F	M	F
Years post disease onset	2	7.5	3
Age (years)	69	59	71
Language severity (FTD-CDR)	2	2	2
Total severity (FTD-CDR)	10	5.5	5
Letter fluency (total words)	4	27	12
Semantic fluency (total words)	6	9	18
Digit span forward (total digits)	3	7	3
Digit span backward (total digits)	2	6.5	2.5
Spatial span forward (total digits)	3.5	6	3
Spatial span backward (total digits)	3.5	6	4
Sentence anagrams (correct of 10)	4	10	5
Sentence repetition (correct of 37)	31	35	24
Boston naming test (correct of 30)	18	1	16
Hopkins assessment for naming actions (correct of 35)	14	6	15
S.O.A.P. syntactic comprehension (correct of 40)	8	39	9
Rey auditory verbal learning, sum of trials 1–5 (75 possible)	65	30	8
Trail-making test A (time in sec)	57	36	39
Trail-making test B (time in sec)	219	52	169

applied to the distal surface of the effective "cathode" electrode, and (3) all other external surfaces treated as insulated. The induced cortical electric field was calculated as a result of a tDCS montage intended to influence the left inferior frontal gyrus (IFG) area (for rectangular-pad stimulation: 5×5 cm^2 sponges, anode: F7, cathode: zygoma) (Fig. 1). In order to implement the concentric-ring configuration [29], we simulated 5 HD electrodes (5 mm radius) in a ring with four "return" (cathode) disc electrodes around (4 cm electrode center-to-center ring radius) around an "active" (anode) center electrode over left IFG area (coinciding with the center of the active pad used for rectangular-pad stimulation).

Radial electric field was calculated as the component of the electric field on the brain surface in the direction normal to the surface [29]. The minimum brain to skull distance specifically for gyri and sulci measurements was based on the distance of the test surface (skull) to the reference surface (whole gray matter, gyri-only, sulci-only) by measuring the minimum distance from each element on reference surfaces to the nearest element on the test surface. The rationale for separately considering gyri-only and sulci-only surfaces (in addition to all of gray matter) was as follows. In visualizing the interaction between skull-brain distance and electric fields, when considering all of gray matter, essentially all gyri crowns appear as one extreme (e.g., blue) and gyri as another extreme (e.g., red), while independent visualization of gyri-only or sulci-only features allows consideration of nuanced changes among the most superficial or among more deep brain layers, respectively. Statistics (mean deviation and mean positive and negative deviations) are calculated as weighted averages of values obtained at individual vertices of the reference surface, with the weight of each vertex proportional to the area of the Voronoi cell containing that vertex [33].

Results

For the conventional 5×5 cm^2 pad tDCS and the 4×1 ring HD-tDCS configurations, we calculated the induced cortical electric field (EF) across three subjects with PPA. The cortical

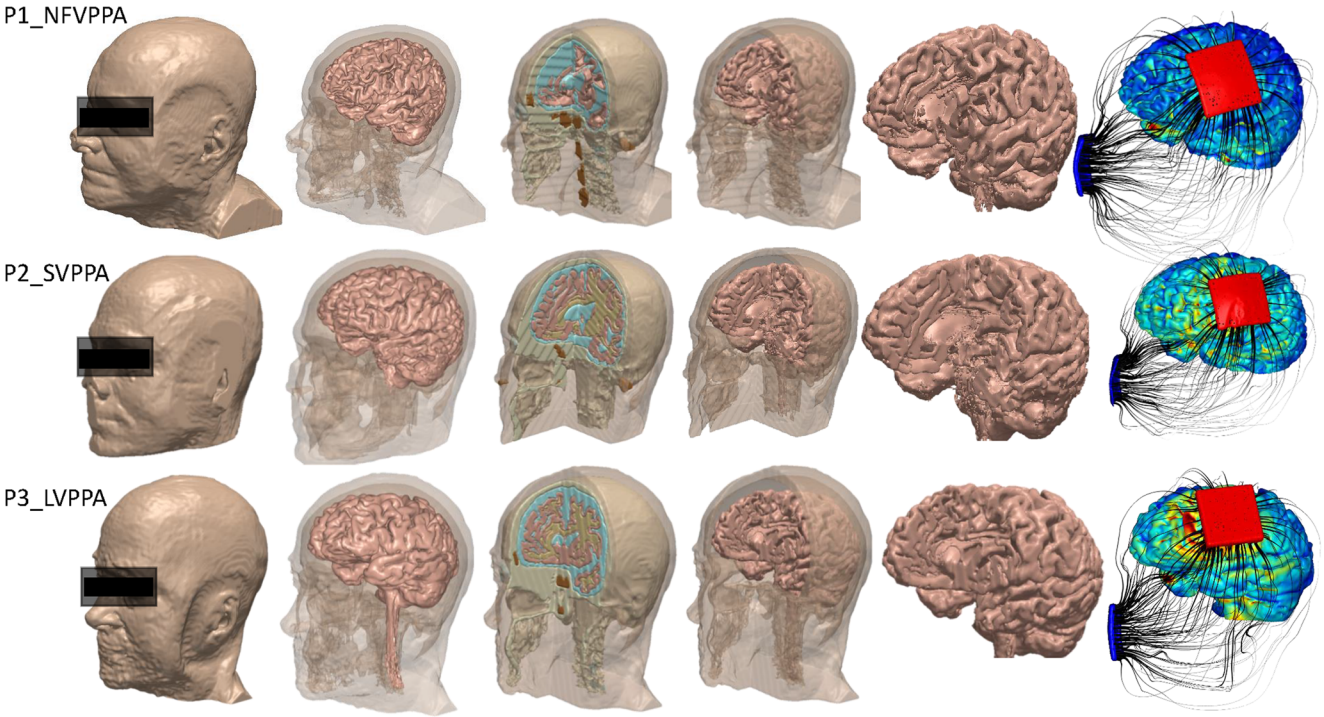

Fig. 1 High-resolution tDCS modeling in primary progressive aphasia (PPA). T1- and T2-weighted sequence MRIs were collected at a resolution of 1 mm. Three subjects, each representing one variant of PPA, i.e., semantic variant PPA, non-fluent variant PPA, and logopenic variant PPA that have different patterns of atrophy, were segmented into six tissue compartments (i.e., skin, skull, gray matter, white matter, cerebrospinal fluid, and air) using automated algorithm and manual segmentation techniques. Special attention was paid to correct segmentation of brain atrophy. Current flow through each head was simulated using FEM to predict cortical electric field

electric field (EF) plots for each montage and subject were considered against local anatomical metrics of bone-gray matter distance, bone-sulci distance, or bone-gyri distance (see the "Methods" section).

Conventional tDCS pad current flow

Conventional pad stimulation resulted in current clustering with diffuse modulation over wide parts of the cortex (Fig. 2). Consistent with previous predictions, the overall current flow was complex, reflecting the convoluted gyri-sulci morphology and individual neuroanatomy [5, 18, 34].

As expected from prior studies [6, 10], tDCS across subjects resulted in different electric field distributions. Generally, maximal brain current flow, as reflected in clustering of peak electric field, was predicted in brain regions broadly spanning between the two electrodes, but the location of specific electric field peaks was idiosyncratic. For 2 mA stimulation, peak (brain wide) electric field across subjects was 0.55 V/m (P1_nfvPPA), 0.55 V/m (P2_svPPA), and 0.70 V/m (P3_lvPPA). These peaks reflect a very small region of cortex; to facilitate comparison, electric field magnitude and radial plots are two similar scales (Fig. 2). As expected, radial electric fields distribution generally tracked electric magnitude in diffusivity and clustering (i.e., significant radial electric fields require significant electric field magnitude [35–38]). Consistent with prior models of individuals with normal anatomy [39], radial field direction alternated across the cortical surface, often across individual gyri with inward current on side of a gyri and outward current on the opposite side.

High-definition tDCS

For each subject, the 4 × 1 ring HD-tDCS montage resulted in a cortical activation area circumscribed by the ring, thereby leading to significant focality increases (Fig. 2, electric field (4 × 1)). There was no significant current flow modulation in the prefrontal, contralateral, or occipital areas. Differences in peak magnitudes across subjects were predicted; however, the location of the peak electric field was consistently at the 4 × 1 ring.

Bone-gray matter (including bone-sulci and bone-gyri) distance

The aim of measuring bone-gray matter distance was to correlate local electric field distribution or radial electric fields with local morphological features of the cortex. However, no correlation was evidenced across any measures that explained patterns within subjects or the difference across subjects for either conventional or HD-tDCS. For example, considering

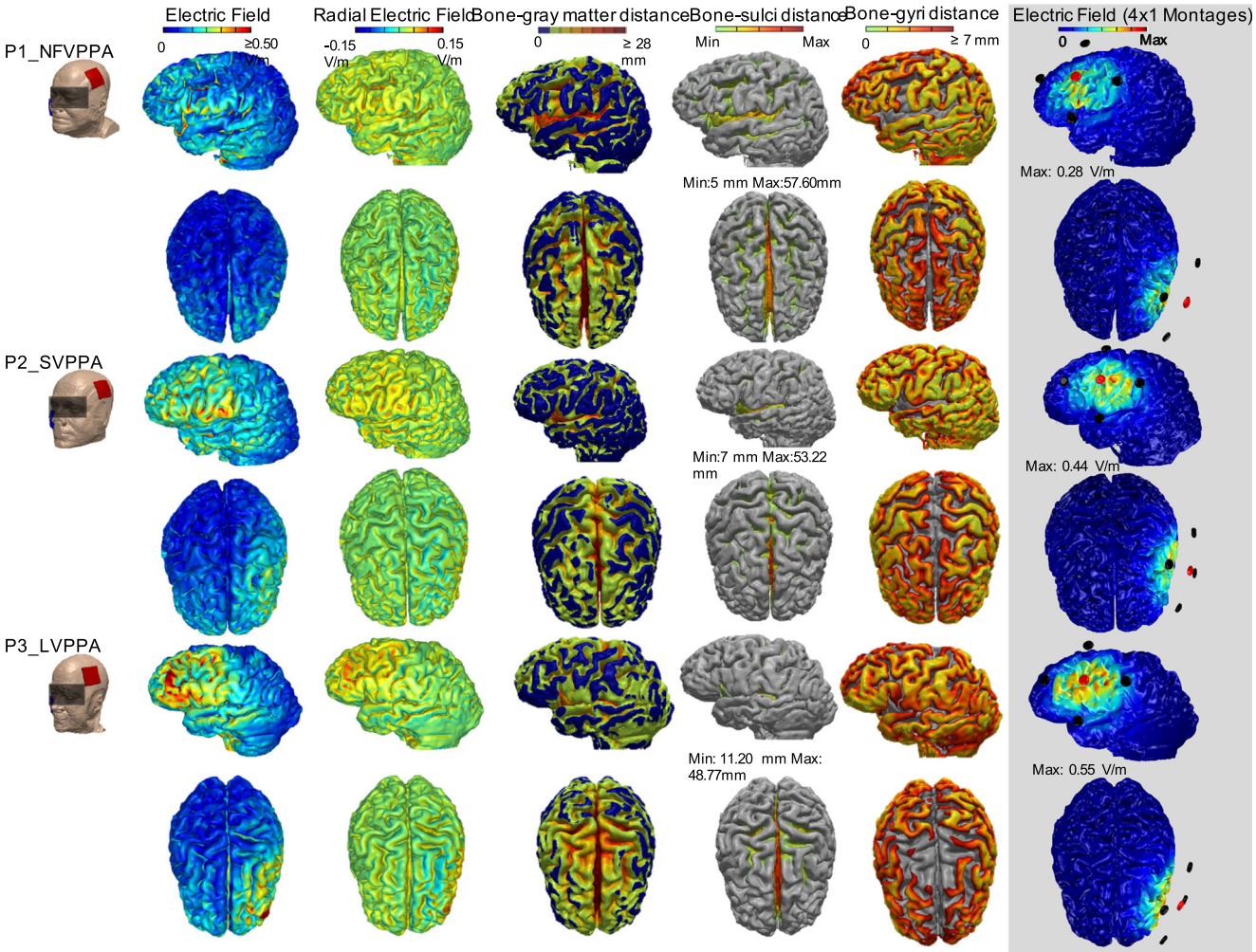

Fig. 2 Current flow during tDCS and cortical anatomy in the exemplary cases of three subjects with primary progressive aphasia (P1_NFVPPA, P2_SVPPA, and P3_LVPPA). (first column) Electrode montage on three subjects. (second column) Electric field magnitude on cortical surface in lateral (top) and superior (bottom) view. False color map: red ≥ 0.5 V/m, blue 0 V/m. (third column) Electric field normal to the cortical surface. False color map: red maximally inward; blue, maximally outward. (fourth column) Minimum distance from cortical gray matter surface to nearest bone. False color map: red ≥ 28 mm, blue 0–3 mm. (fifth column) Minimum distance from sulci to nearest bone. False color map: red, max; green, min. (sixth column) Minimum distance from gyri to nearest bone. False color map: red, ≥ 7 mm; green, 0–2 mm. (seventh column) Electric field for 4 × 1 montage

overall brain surface to skull distance (Fig. 2; bone-gray matter distance), gyri across the brain, especially at lateralized regions, are at the shortest distance range considered (blue; distance < 3 mm); by inspection, the electric field correspondence to this shortest (blue) range varies. This is especially evident in occipital regions where there is minimal electric field regardless of bone-gray matter distance. But even in brain regions under and between stimulation electrodes, the pattern of electric field magnitude or radial electric field peaks is not reliably correlated with minimal bone-gray matter distance.

As expected, the largest range considered for brain surface to skull distance (red; > 22 mm) is seen in the sulci, notably in the lateral sulcus and the longitudinal fissure. This is reinforced when only the distance of the brain sulci to the skull is considered (Fig. 2; bone-sulci distance). Again, no correlation between local anatomy and electric field magnitude or radial electric fields is evident. By inspection, one might note that electric field magnitude may peak in gyri around the lateral sulcus, but not consistently. Finally, focusing only on the gyri crowns (Fig. 2; bone-gyri distance) also fails to reveal any evident correlation with electric field magnitude or radial electric fields.

Comparing across the three types of PPA modeled, there are no evident patterns correlating anatomical measures and electric fields. The clustering of electric fields varies across subjects. While electric field clusters are more likely to be present in the brain areas between electrodes, the location of the peak electric fields is not consistent across each subject (and in no subject under the electrodes). Notably, inter-subject

variance of electric field peak magnitude and distribution are in line with studies in neurologically intact subjects for either conventional or HD-tDCS [6, 10].

Discussion

In this study, we addressed the question whether variant-distinct atrophy patterns affect electrical current distribution in PPA. We developed the first high-resolution models of current flow models of tDCS in three individuals with distinct cortical atrophy patterns of PPA. While the specific pattern (diffuse clustering) and magnitude of cortical electric fields across individuals varied, this variation was within the range of neurotypical individuals [6, 8]. Thus, applying tDCS (either conventional or HD-tDCS) to individuals with moderate cortical atrophy (moderate language and cognitive severity [34]) does not necessarily result in markedly altered current delivery to the brain compared to healthy individuals, providing, of course, that stimulation is not applied over non-existing tissue. Individualized montage to deliver the appropriate dose may not be specifically mandated in this population—any more or less than in neurotypical subjects [13, 40]. This conclusion is based on the exemplary montages and patients considered here, and may not apply for subjects with more severe or bilateral atrophy. In stroke and other brain injuries, dramatic changes in anatomy can characteristically influence current flow [14, 18], and so customized tDCS dose may be more appropriate [17].

Local brain current intensity and direction were considered relevant for tDCS outcomes [41–45] and so is used as a goal for tDCS optimization [46–49]. It is accepted that (1) gross changes in anatomy (e.g., head size) can influence current delivery to the brain [6, 8]; (2) electric field clustering is stereotypically observed at gyri crowns [5] or sulci [4]; (3) current directionality can invert across a gyrus [39]; and (4) the high-conductivity CSF strongly influences these current flow patterns [50]. But the correlation of local brain morphology with electric fields remains unclear [9]. The results of the present study suggest that electric fields are not predicted simply by local measures of morphology such as measures of distance from the skull to the brain (CSF thickness). Adjacent brain regions with comparable morphology often showed very different electric field intensities for both conventional and HD-tDCS.

Rather, our results are consistent with the notion that the current flow in any given brain region is determined by holistic morphology—meaning the morphology and global atrophy of the entire head must be taken into account to explain current flow patterns in each brain region. This is exactly the function of current flow models which are increasingly automated and accessible [3, 51–53]. However, existing automatic segmentation routines may not adequately address mild or moderate atrophy in PPA. While the accuracy of models in regard to gross current flow has been repeatedly validated [10–12], the location and intensity of local maximum are sensitive to modeling details. Therefore, especially in considering the significance of electric field clusters in atypical brains, unknowns about modeling precision that apply even in neurotypical brains should be recognized [54–57]. Generally, open questions remain about the mechanisms of tDCS: (1) how to interpret current flow models for protocol optimization [2, 58–60] and (2) whether the degree of "neuromodulation" simply increases with electric field intensity [61, 62] or with the number of sessions and their spacing over a set of days.

Our results support prior modeling and experiments showing that using a conventional (pad) tDCS montage produces diffuse brain current, with the location of peak electric field varying across subjects; conventional tDCS may leverage circuit therapeutics or be combined with functional targeting. To the extent that clinical outcomes depend on focal stimulation, 4 × 1 HD-tDCS is useful [63]; [5, 13].

We would like to add a final note on clinical outcomes in neurodegenerative conditions and how they may or may not be impacted by the current flow. In our randomized sham-controlled clinical trial, the non-fluent variant of PPA showed the most benefit from tDCS over the left IFG, i.e., tDCS resulted in the highest additional boost of performance in written naming and spelling for both trained and untrained words in comparison to the other variants (the logopenic and the semantic variant of PPA with parieto-temporal and temporal atrophy, respectively) [24]. However, the present study of current modeling did not show any significant differences in electrical current distribution between variants with different atrophy patterns. One possible conclusion is, thus, that atrophy over the stimulated area does not matter for current flow and other factors may be more important for behavioral effects due to tDCS. In a subsequent study, we looked at other language and behavioral predictors of tDCS effects and found that initial task performance was among the strongest predictors of tDCS effects [64]. We have also shown that one of the possible neural mechanisms for tDCS effects is a change in functional connectivity between the targeted area (left IFG) and its structural and functional connections with the areas involved in the task practiced during tDCS [65]. Therefore, functional connectivity of the stimulated area may determine tDCS effects more than atrophy. In support of this hypothesis, a recent study using graph theory has shown that frontal atrophy did not correlate with functional connectivity in nfvPPA [66].

Alternatively, we need to entertain two other logical hypotheses: (1) the current may have stimulated other areas, probably in the vicinity of the targeted area, that are important for lexical retrieval, or (2) the left IFG had changed topography but was nevertheless adequately reached by the diffuse

current, probably because of the diffuse current distribution. Although we cannot completely exclude the first hypothesis, there is strong scientific evidence that the left IFG and in particular the left IFG triangularis is a neural substrate for lexical retrieval [67, 68]. Of course, we cannot exclude the hypothesis that the improvement in lexical retrieval was due to the improvement in other functions of the frontal operculum, such as monitoring. As for the second hypothesis, the above-mentioned study [66] showed that nfvPPA is associated with network-specific topological alterations with loss of hubs in the left frontoparietal-temporal area. Therefore, the functions of the left IFG may have "migrated" to neighboring areas of the left frontal operculum that were reached by the electrical current of the large electrode patches used. If this hypothesis is correct, then further studies would need to estimate whether functional connectivity correlates with current flow patterns. If brain functional connectivity topography changes in neurodegeneration, then electrical current diffusivity may not work against, and may actually promote, the therapeutic effects of tDCS, but this is an empirical question for further research. Another hypothesis generated by the present study is that HD-tDCS montages, targeting the left IFG triangularis in particular, will induce even larger behavioral effects in lexical retrieval. Future research is needed to compare the two types of montages for the same function (e.g., lexical retrieval) to answer this question.

Acknowledgments We would like to thank our participants and referring physicians for their dedication and interest in our study.

Funding information This work was supported through the National Institutes of Health: NIH–NINDS 1R01NS101362, NIH–NIMH 1R01MH111896 to MB and by the National Institutes of Health (National Institute of Deafness and Communication Disorders) through award R01 DC014475 to KT.

Compliance with ethical standards

Conflict of interest The City University of New York has patents on Brain Stimulation with MB as inventor. MB has equity in Soterix Medical and serves on the Boston Scientific and GlaxoSmithKline scientific advisory boards.

Ethical approval The study was approved by Johns Hopkins University IRB.

References

1. Peterchev AV, Wagner TA, Miranda PC, Nitsche MA, Paulus W, Lisanby SH, Pascual-Leone A, Bikson M (2012) Fundamentals of transcranial electric and magnetic stimulation dose: definition, selection, and reporting practices. Brain Stimul 5:435–453. https://doi.org/10.1016/j.brs.2011.10.001
2. Ruffini G, Wendling F, Merlet I, Molaee-Ardekani B, Mekonnen A, Salvador R, Soria-Frisch A, Grau C, Dunne S, Miranda PC (2013) Transcranial current brain stimulation (tCS): models and technologies. IEEE Trans Neural Syst Rehabil Eng 21:333–345. https://doi.org/10.1109/TNSRE.2012.2200046
3. Miranda PC (2013) Physics of effects of transcranial brain stimulation. Handb Clin Neurol 116:353–366. https://doi.org/10.1016/B978-0-444-53497-2.00029-2
4. Miranda PC, Lomarev M, Hallett M (2006) Modeling the current distribution during transcranial direct current stimulation. Clin Neurophysiol 117:1623–1629. https://doi.org/10.1016/j.clinph.2006.04.009
5. Datta A, Bansal V, Diaz J, et al (2009) Gyri-precise head model of transcranial direct current stimulation: improved spatial focality using a ring electrode versus conventional rectangular pad. Brain Stimul 2:201–207, 207.e1
6. Datta A, Truong D, Minhas P et al (2012) Inter-individual variation during transcranial direct current stimulation and normalization of dose using MRI-derived computational models. Front Psychiatry 3:91. https://doi.org/10.3389/fpsyt.2012.00091
7. Parazzini M, Fiocchi S, Rossi E, Paglialonga A, Ravazzani P (2011) Transcranial direct current stimulation: estimation of the electric field and of the current density in an anatomical human head model. IEEE Trans Biomed Eng 58:1773–1780. https://doi.org/10.1109/TBME.2011.2116019
8. Truong DQ, Magerowski G, Blackburn GL, Bikson M, Alonso-Alonso M (2013) Computational modeling of transcranial direct current stimulation (tDCS) in obesity: impact of head fat and dose guidelines. NeuroImage: Clinical 2:759–766. https://doi.org/10.1016/j.nicl.2013.05.011
9. Opitz A, Paulus W, Will S, Antunes A, Thielscher A (2015) Determinants of the electric field during transcranial direct current stimulation. NeuroImage 109:140–150. https://doi.org/10.1016/j.neuroimage.2015.01.033
10. Huang Y, Liu AA, Lafon B et al (2017) Measurements and models of electric fields in the in vivo human brain during transcranial electric stimulation. Elife 6. https://doi.org/10.7554/eLife.18834
11. Jog MV, Smith RX, Jann K, Dunn W, Lafon B, Truong D, Wu A, Parra L, Bikson M, Wang DJ (2016) In-vivo imaging of magnetic fields induced by transcranial direct current stimulation (tDCS) in human brain using MRI. Sci Rep 6:34385. https://doi.org/10.1038/srep34385
12. Datta A, Zhou X, Su Y, Parra LC, Bikson M (2013) Validation of finite element model of transcranial electrical stimulation using scalp potentials: implications for clinical dose. J Neural Eng 10:036018. https://doi.org/10.1088/1741-2560/10/3/036018
13. Edwards D, Cortes M, Datta A, Minhas P, Wassermann EM, Bikson M (2013) Physiological and modeling evidence for focal transcranial electrical brain stimulation in humans: a basis for high-definition tDCS. NeuroImage 74:266–275. https://doi.org/10.1016/j.neuroimage.2013.01.042
14. Datta A, Bikson M, Fregni F (2010) Transcranial direct current stimulation in patients with skull defects and skull plates: high-resolution computational FEM study of factors altering cortical current flow. Neuroimage 52:1268–1278
15. Tomio R, Akiyama T, Horikoshi T et al (2015) Visualization of the electric field evoked by transcranial electric stimulation during a craniotomy using the finite element method. J Neurosci Methods 256:157–167. https://doi.org/10.1016/j.jneumeth.2015.09.014
16. Gillick BT, Kirton A, Carmel JB, Minhas P, Bikson M (2014) Pediatric stroke and transcranial direct current stimulation: methods for rational individualized dose optimization. Front Hum Neurosci 8:739. https://doi.org/10.3389/fnhum.2014.00739
17. Dmochowski JP, Datta A, Huang Y, Richardson JD, Bikson M, Fridriksson J, Parra LC (2013) Targeted transcranial direct current stimulation for rehabilitation after stroke. Neuroimage 75:12–19. https://doi.org/10.1016/j.neuroimage.2013.02.049
18. Datta A, Baker JM, Bikson M, Fridriksson J (2011) Individualized model predicts brain current flow during transcranial direct-current

stimulation treatment in responsive stroke patient. Brain Stimulation 4:169–174. https://doi.org/10.1016/j.brs.2010.11.001
19. Galletta EE, Cancelli A, Cottone C, Simonelli I, Tecchio F, Bikson M, Marangolo P (2015) Use of computational modeling to inform tDCS electrode montages for the promotion of language recovery in post-stroke aphasia. Brain Stimul 8:1108–1115. https://doi.org/10.1016/j.brs.2015.06.018
20. Ciechanski P, Carlson HL, Yu SS, Kirton A (2018) Modeling transcranial direct-current stimulation-induced electric fields in children and adults. Front Hum Neurosci 12:268. https://doi.org/10.3389/fnhum.2018.00268
21. Minhas P, Bikson M, Woods AJ, et al (2012) Transcranial direct current stimulation in pediatric brain: a computational modeling study. In: 2012 Annual International Conference of the IEEE Engineering in Medicine and Biology Society. Pp 859–862
22. Teichmann M, Lesoil C, Godard J, Vernet M, Bertrand A, Levy R, Dubois B, Lemoine L, Truong DQ, Bikson M, Kas A, Valero-Cabré A (2016) Direct current stimulation over the anterior temporal areas boosts semantic processing in primary progressive aphasia. Ann Neurol 80:693–707. https://doi.org/10.1002/ana.24766
23. Fridriksson J, den Ouden D-B, Hillis AE et al (2018) Anatomy of aphasia revisited. Brain 141:848–862
24. Tsapkini K, Webster KT, Ficek BN, Desmond JE, Onyike CU, Rapp B, Frangakis CE, Hillis AE (2018) Electrical brain stimulation in different variants of primary progressive aphasia: a randomized clinical trial. Alzheimers Dement (N Y) 4:461–472. https://doi.org/10.1016/j.trci.2018.08.002
25. Gorno-Tempini ML, Hillis AE, Weintraub S, Kertesz A, Mendez M, Cappa SF, Ogar JM, Rohrer JD, Black S, Boeve BF, Manes F, Dronkers NF, Vandenberghe R, Rascovsky K, Patterson K, Miller BL, Knopman DS, Hodges JR, Mesulam MM, Grossman M (2011) Classification of primary progressive aphasia and its variants. Neurology 76:1006–1014
26. Mesulam M, Wieneke C, Rogalski E, Cobia D, Thompson C, Weintraub S (2009) Quantitative template for subtyping primary progressive aphasia. Arch Neurol 66:1545–1551
27. Cotelli M, Manenti R, Paternicò D, Cosseddu M, Brambilla M, Petesi M, Premi E, Gasparotti R, Zanetti O, Padovani A, Borroni B (2016) Grey matter density predicts the improvement of naming abilities after tDCS intervention in agrammatic variant of primary progressive aphasia. Brain Topogr 29:738–751
28. de Aguiar V, Zhao Y, Faria A, et al (under review) Brain volumes as predictors of electrical stimulation effects in primary progressive aphasia
29. Datta A, Elwassif M, Battaglia F, Bikson M (2008) Transcranial current stimulation focality using disc and ring electrode configurations: FEM analysis. J Neural Eng 5:163–174. https://doi.org/10.1088/1741-2560/5/2/007
30. Huang Y, Datta A, Bikson M, Parra LC (2017) Realistic volumetric-approach to simulate transcranial electric stimulation – ROAST – a fully automated open-source pipeline bioRxiv 217331. https://doi.org/10.1101/217331
31. Ashburner J, Friston KJ (2005) Unified segmentation. Neuroimage 26:839–851. https://doi.org/10.1016/j.neuroimage.2005.02.018
32. Huang Y, Dmochowski JP, Su Y, Datta A, Rorden C, Parra LC (2013) Automated MRI segmentation for individualized modeling of current flow in the human head. J Neural Eng 10:066004. https://doi.org/10.1088/1741-2560/10/6/066004
33. Ghosh S, Moorthy S (1995) Elastic-plastic analysis of arbitrary heterogeneous materials with the Voronoi cell finite element method. Comput Methods Appl Mech Eng 121:373–409. https://doi.org/10.1016/0045-7825(94)00687-I
34. Knopman DS, Kramer JH, Boeve BF, Caselli RJ, Graff-Radford NR, Mendez MF, Miller BL, Mercaldo N (2008) Development of methodology for conducting clinical trials in frontotemporal lobar degeneration. Brain 131:2957–2968
35. Seo H, Kim D, Jun SC (2015) Computational study of subdural cortical stimulation: effects of simulating anisotropic conductivity on activation of cortical neurons. PLoS One 10:e0128590
36. Waters S, Wiestler T, Diedrichsen J (2017) Cooperation not competition: bihemispheric tDCS and fMRI show role for ipsilateral hemisphere in motor learning. J Neurosci 37:7500–7512
37. Petrov PI, Mandija S, Sommer IE et al (2017) How much detail is needed in modeling a transcranial magnetic stimulation figure-8 coil: measurements and brain simulations. PLoS One 12:e0178952
38. Bonaiuto JJ, de Berker A, Bestmann S (2016) Response repetition biases in human perceptual decisions are explained by activity decay in competitive attractor models. Elife 5:e20047
39. Lafon B, Rahman A, Bikson M, Parra LC (2017) Direct current stimulation alters neuronal input/output function. Brain Stimul 10:36–45. https://doi.org/10.1016/j.brs.2016.08.014
40. Laakso I, Tanaka S, Koyama S et al (2015) Inter-subject variability in electric fields of motor cortical tDCS. Brain Stimulation. https://doi.org/10.1016/j.brs.2015.05.002
41. Rawji V, Ciocca M, Zacharia A, Soares D, Truong D, Bikson M, Rothwell J, Bestmann S (2018) tDCS changes in motor excitability are specific to orientation of current flow. Brain Stimul 11:289–298. https://doi.org/10.1016/j.brs.2017.11.001
42. Salvador R, Wenger C, Miranda PC (2015) Investigating the cortical regions involved in MEP modulation in tDCS Front Cell Neurosci 9:. https://doi.org/10.3389/fncel.2015.00405
43. Mikkonen M, Laakso I, Sumiya M, Koyama S, Hirata A, Tanaka S (2018) TMS motor thresholds correlate with TDCS electric field strengths in hand motor area. Front Neurosci 12:426. https://doi.org/10.3389/fnins.2018.00426
44. Rahman A, Reato D, Arlotti M, Gasca F, Datta A, Parra LC, Bikson M (2013) Cellular effects of acute direct current stimulation: somatic and synaptic terminal effects. J Physiol 591:2563–2578. https://doi.org/10.1113/jphysiol.2012.247171
45. Kabakov AY, Muller PA, Pascual-Leone A, Jensen FE, Rotenberg A (2012) Contribution of axonal orientation to pathway-dependent modulation of excitatory transmission by direct current stimulation in isolated rat hippocampus. J Neurophysiol 107:1881–1889. https://doi.org/10.1152/jn.00715.2011
46. Dmochowski JP, Datta A, Bikson M, Su Y, Parra LC (2011) Optimized multi-electrode stimulation increases focality and intensity at target. J Neural Eng 8:046011. https://doi.org/10.1088/1741-2560/8/4/046011
47. Miranda PC, Salvador R, Wenger C, Fernandes SR (2017) Optimizing electric-field delivery for tDCS: virtual humans help to design efficient, noninvasive brain and spinal cord electrical stimulation. IEEE Pulse 8:42–45. https://doi.org/10.1109/MPUL.2017.2701259
48. Bikson M, Dmochowski J, Rahman A (2013) The "quasi-uniform" assumption in animal and computational models of non-invasive electrical stimulation. Brain Stimul 6:704–705. https://doi.org/10.1016/j.brs.2012.11.005
49. Bikson M, Truong DQ, Mourdoukoutas AP, et al (2015) Chapter 1 - Modeling sequence and quasi-uniform assumption in computational neurostimulation. In: Bestmann S (ed) Progress in Brain Research. Elsevier, pp 1–23
50. Wagner S, Rampersad SM, Aydin Ü, Vorwerk J, Oostendorp TF, Neuling T, Herrmann CS, Stegeman DF, Wolters CH (2014) Investigation of tDCS volume conduction effects in a highly realistic head model. J Neural Eng 11:016002. https://doi.org/10.1088/1741-2560/11/1/016002
51. Huang Y, Datta A, Bikson M, Parra LC (2018) ROAST: an open-source, fully-automated, realistic volumetric-approach-based simulator for TES. Conf Proc IEEE Eng Med Biol Soc 2018:3072–3075. https://doi.org/10.1109/EMBC.2018.8513086
52. Thielscher A, Antunes A, Saturnino GB (2015) Field modeling for transcranial magnetic stimulation: a useful tool to understand the

physiological effects of TMS? In: 2015 37th Annual International Conference of the IEEE Engineering in Medicine and Biology Society (EMBC). Pp 222–225
53. Truong DQ, Hüber M, Xie X, Datta A, Rahman A, Parra LC, Dmochowski JP, Bikson M (2014) Clinician accessible tools for GUI computational models of transcranial electrical stimulation: BONSAI and SPHERES. Brain Stimul 7:521–524. https://doi.org/10.1016/j.brs.2014.03.009
54. Shahid SS, Bikson M, Salman H, Wen P, Ahfock T (2014) The value and cost of complexity in predictive modelling: role of tissue anisotropic conductivity and fibre tracts in neuromodulation. J Neural Eng 11:036002. https://doi.org/10.1088/1741-2560/11/3/036002
55. Bikson M, Datta A (2012) Guidelines for precise and accurate computational models of tDCS. Brain Stimulation 5:430–431. https://doi.org/10.1016/j.brs.2011.06.001
56. Santos L, Martinho M, Salvador R et al (2016) Evaluation of the electric field in the brain during transcranial direct current stimulation: a sensitivity analysis. Conf Proc IEEE Eng Med Biol Soc 2016:1778–1781. https://doi.org/10.1109/EMBC.2016.7591062
57. Miranda PC, Salvador R, Wenger C, Fernandes SR (2016) Computational models of non-invasive brain and spinal cord stimulation. Conf Proc IEEE Eng Med Biol Soc 2016:6457–6460. https://doi.org/10.1109/EMBC.2016.7592207
58. de Berker AO, Bikson M, Bestmann S (2013) Predicting the behavioral impact of transcranial direct current stimulation: issues and limitations. Front Hum Neurosci 7:613. https://doi.org/10.3389/fnhum.2013.00613
59. Bestmann S, Ward N (2017) Are current flow models for transcranial electrical stimulation fit for purpose? Brain Stimul 10:865–866. https://doi.org/10.1016/j.brs.2017.04.002
60. Molaee-Ardekani B, Márquez-Ruiz J, Merlet I et al (2013) Effects of transcranial direct current stimulation (tDCS) on cortical activity: a computational modeling study. Brain Stimulation 6:25–39. https://doi.org/10.1016/j.brs.2011.12.006
61. Bonaiuto JJ, Bestmann S (2015) Understanding the nonlinear physiological and behavioral effects of tDCS through computational neurostimulation. Prog Brain Res 222:75–103. https://doi.org/10.1016/bs.pbr.2015.06.013
62. Esmaeilpour Z, Marangolo P, Hampstead BM, Bestmann S, Galletta E, Knotkova H, Bikson M (2018) Incomplete evidence that increasing current intensity of tDCS boosts outcomes. Brain Stimul 11:310–321. https://doi.org/10.1016/j.brs.2017.12.002
63. Kuo H-I, Bikson M, Datta A, Minhas P, Paulus W, Kuo MF, Nitsche MA (2013) Comparing cortical plasticity induced by conventional and high-definition 4 × 1 ring tDCS: a neurophysiological study. Brain Stimulation 6:644–648. https://doi.org/10.1016/j.brs.2012.09.010
64. de Aguiar V, Zhao Y, Ficek B, et al (under review) Predictors of the effects of spelling intervention and tDCS in primary progressive aphasia
65. Ficek BN, Wang Z, Zhao Y, et al (2018) The effect of tDCS on functional connectivity in primary progressive aphasia. NeuroImage: Clinical. https://doi.org/10.1016/j.nicl.2018.05.023
66. Mandelli ML, Welch AE, Vilaplana E, Watson C, Battistella G, Brown JA, Possin KL, Hubbard HI, Miller ZA, Henry ML, Marx GA, Santos-Santos MA, Bajorek LP, Fortea J, Boxer A, Rabinovici G, Lee S, Deleon J, Rosen HJ, Miller BL, Seeley WW, Gorno-Tempini ML (2018) Altered topology of the functional speech production network in non-fluent/agrammatic variant of PPA. Cortex 108:252–264. https://doi.org/10.1016/j.cortex.2018.08.002
67. Petrides M, Alivisatos B, Evans AC (1995) Functional activation of the human ventrolateral frontal cortex during mnemonic retrieval of verbal information. Proc Natl Acad Sci U S A 92:5803–5807
68. Thompson-Schill SL, D'Esposito M, Aguirre GK, Farah MJ (1997) Role of left inferior prefrontal cortex in retrieval of semantic knowledge: a reevaluation. Proc Natl Acad Sci 94:14792–14797
69. Benton AL, Sivan AB, deS Hamsher K, Spreen O (1994) Contributions to neuropsychological assessment: a clinical manual. Oxford University Press, USA
70. Wechsler D (1981) Manual for the Wechsler adult intelligence scale-revised (WAIS-R). San Antonio, TX: The Psychological Corporation
71. Kaplan E (1983) The assessment of aphasia and related disorders. Lippincott Williams & Wilkins
72. Breining BL, Tippett DC, Posner J, et al (2015) Assessing dissociations of object and action naming in acute stroke. In: Clinical Aphasiology Conference, Monterey, CA
73. Love T, Oster E (2002) On the categorization of aphasic typologies: the SOAP (a test of syntactic complexity). J Psycholinguist Res 31:503–529. https://doi.org/10.1023/A:1021208903394